




ORIGINAL ARTICLE

Triphilic pentablock copolymers with perfluoroalkyl segment in central position

Daniel Heinz¹ | Annette Meister¹  | Hazrat Hussain² | Karsten Busse¹  | Jörg Kressler¹ 

¹Department of Chemistry, Martin Luther University Halle-Wittenberg, Halle (Saale), Germany

²Department of Chemistry, Quaid-i-Azam University, Islamabad, Pakistan

Correspondence

Jörg Kressler, Department of Chemistry, Martin Luther University Halle-Wittenberg, D-06099 Halle (Saale), Germany.
Email: joerg.kressler@chemie.uni-halle.de

Funding information

Alexander von Humboldt-Stiftung; Deutsche Forschungsgemeinschaft, Grant/Award Number: FOR-1145

Abstract

Adding perfluoroalkyl (PF) segments to amphiphilic copolymers yields triphilic copolymers with new application profiles. Usually, PF segments are attached as terminal blocks via Cu(I) catalyzed azide-alkyne cycloaddition (CuAAC). The purpose of the current study is to design new triphilic architectures with a PF segment in central position. The PF segment bearing bifunctional atom transfer radical polymerization (ATRP) initiator is employed for the fabrication of triphilic poly(propylene oxide)-*b*-poly(glycerol monomethacrylate)-*b*-PF-*b*-poly(glycerol monomethacrylate)-*b*-poly(propylene oxide) PPO-*b*-PGMA-*b*-PF-*b*-PGMA-*b*-PPO pentablock copolymers by a combined ATRP and CuAAC reaction approach. Differential scanning calorimetry indicates the PF-initiator to undergo a solid–solid phase transition at 63°C before the final crystal melting at 95°C. This is further corroborated by polarized optical microscopy and X-ray diffraction studies. The PF-initiator could successfully polymerize solketal methacrylate (SMA) under typical ATRP conditions producing well-defined Br-PSMA-*b*-PF-*b*-PSMA-Br triblock copolymers that are then converted into PPO-*b*-PSMA-*b*-PF-*b*-PSMA-*b*-PPO pentablock copolymer via CuAAC reaction. Subsequently, acid hydrolysis of the PSMA blocks afforded water soluble well-defined triphilic pentablock copolymers PPO-*b*-PGMA-*b*-PF-*b*-PGMA-*b*-PPO with fluorophilic central segment, hydrophilic middle blocks, and lipophilic outer blocks. The triphilic block copolymers could self-assemble, depending upon the preparatory protocol, into spherical and filament-like phase-separated nanostructures as revealed by transmission electron microscopy.

KEYWORDS

ATRP, CuAAC, fluoropolymer, self-assembly, triphilic block copolymers

1 | INTRODUCTION

Triphilic polymers having hydrophilic, lipophilic, and fluorophilic segments represent an extension of the

concept of amphiphilic polymers.^{1–8} The introduction of fluorophilic segments, which are neither hydrophilic nor lipophilic increases the structural diversity of block copolymers in bulk and in selective solvents dramatically.^{9–13}

This is an open access article under the terms of the Creative Commons Attribution License, which permits use, distribution and reproduction in any medium, provided the original work is properly cited.

© 2020 The Authors. *Journal of Polymer Science* published by Wiley Periodicals LLC.

Triphilic block copolymers have been reported to form an incredible array of self-assembled nanostructured morphologies in selective solvents, ranging from typical core-shell-corona micelles,^{2,14} multicompartment micelles,^{2,4,7,15,16} nanocapsules,^{1,6,17} and many more.^{1,18–24} One of the main motivations of studying these unique nanostructures is the possibility of selective storage and delivery of incompatible ingredients/drugs and subsequent controlled release of the payload for potential biomedical applications.²⁵ More recently, Houvenagel et al.²⁶ reported the fabrication of nanocapsules as delivery vehicles for ultrasound contrast agents fabricated from comb-like triphilic polymers. Kaberov et al.²⁷ investigated poly(2-oxazoline)-based triphilic block copolymers as contrast agents for magnetic resonance imaging (MRI).

Previously, extensive studies have been reported on syntheses and nanostructure formation of triphilic linear ABC and miktoarm star ABC block copolymers in solution. Surprisingly, little attention has been paid to symmetric CBABC linear pentablock copolymers.^{28–30} In a previous study, we reported on symmetric CBABC type triphilic pentablock copolymers with terminal perfluoroalkyl (PF) (fluorophilic) segment, middle poly(glycerol monomethacrylate) (PGMA) (hydrophilic), and central poly(propylene oxide) (PPO) as the lipophilic block (PF-*b*-PGMA-*b*-PPO-*b*-PGMA-*b*-PF) with their unique phase separated nanostructures in aqueous solution.^{2,30} Especially, controlled radical polymerization (CRP) techniques (also called reversible-deactivation radical polymerization [RDRP]) are powerful tools for the synthesis of segmented copolymers with different architectures and philicities.³¹ With respect to pharmaceutical and biomedical applications it should be mentioned that especially metal-free CRP techniques are suitable for toxicity reasons. Important developments in this field are organocatalyzed ATRP^{32,33} and photoinduced electron transfer reversible addition-fragmentation chain-transfer (PET-RAFT) polymerization.³⁴ Recently, sequence encoded hydrophobic initiators have been employed to tailor the self-assembly and stimuli-responsiveness of hydrophilic telechelics.³⁵ Herein, we describe a new design of symmetric linear pentablock copolymers by employing a bifunctional perfluoroalkyl PF-initiator for atom transfer radical polymerization (ATRP) to synthesize triphilic PPO-*b*-PGMA-*b*-PF-*b*-PGMA-*b*-PPO pentablock copolymers by a combined ATRP and Cu(I) catalyzed azide-alkyne cycloaddition (CuAAC) approach. To the best of our knowledge, a fluorophilic PF-initiator is used for the first time to synthesize triphilic block copolymers with the PF segment in the center of the polymer backbone. Using differential scanning calorimetry (DSC) and wide-angle X-ray diffraction, it was found that the PF-initiator undergoes a solid–solid phase transition before melting.

In contrast, the triphilic block copolymers were completely amorphous in bulk and able to form phase-separated nanostructures of various morphologies after drying from solution studied by transmission electron microscopy (TEM).

2 | EXPERIMENTAL

2.1 | Materials

All chemicals were used as received if not otherwise mentioned. 1*H*,1*H*,12*H*,12*H*-Perfluoro-1,12-dodecanediol (96%), methacrylic acid (99%, stabilized with 100–250 ppm hydroquinone), and 5-hexynoic acid (97%) were purchased from abcr, Germany. Triethylamine (TEA) (99.5%), 2-bromoisobutryl bromide (98%), solketal (98%), PPO monobutyl ether, sodium azide ($\geq 99.0\%$), Cu(I)Br ($\geq 98.0\%$), α,α,α -trifluorotoluene ($\geq 99\%$, dry), and 2,2'-bipyridine (bpy, $\geq 98.0\%$) were purchased from Sigma-Aldrich, Germany. Acetonitrile ($\geq 99.9\%$ [≤ 10 ppm H₂O]), dichloromethane (DCM, $\geq 99.8\%$ [≤ 50 ppm H₂O]), *N,N'*-dicyclohexylcarbodiimide ($\geq 98\%$), *N,N'*-diisopropylcarbodiimide (DCI, $\geq 99\%$), and 4-(dimethylamino)pyridine (DMAP, $\geq 99\%$) were received from Carl Roth, Germany. Oxalic acid was purchased from Laborchemie Apolda, Germany. The deuterated solvents, CDCl₃, and DMSO-*d*₆ were purchased from ARMAR, Germany, and D₂O from Berlin-Chemie, Germany. THF was received from VWR, Germany and distilled over CaH₂ (Fluka, Germany). Solketal methacrylate (SMA) was synthesized according to the procedure described in the Supporting Information S1-S4.

3 | METHODS

3.1 | NMR spectroscopy

Solution nuclear magnetic resonance (NMR) spectra were recorded at 27°C with an Agilent Technologies 500 MHz DD2 spectrometer. The ¹H, ¹³C, and ¹⁹F NMR spectra were recorded with frequencies of 500 MHz, 125 MHz (proton decoupled), and 470 MHz, respectively. The calibration of ¹H and ¹³C chemical shifts follows the signal of the residual solvent to TMS, and for ¹⁹F spectra relative to CFCl₃.³⁶

3.2 | FTIR spectroscopy

The polymer powder was pressed together with KBr to form a tablet. The spectra were recorded with a Bruker Tensor VERTEX 70 spectrometer.

3.3 | Gel permeation chromatography

Gel permeation chromatography (GPC) measurements were performed at 25°C using a Viscotek GPC max setup including a PSS PolarSil column (Polymer Standards Service, 300 Å, 5 µm, 8 × 300 mm) and a refractive index detector. Dimethylformamide (DMF) containing 10 mM LiBr was used as the eluent with a flow rate of 1 ml/min. Poly(methyl methacrylate) (PMMA) standards in the range from 1850 to 342,900 g/mol were used for calibration.

3.4 | DSC measurements

For DSC measurements, 5–10 mg of the sample was filled into an aluminum pan. The measurement was carried out using the DSC 822° module from Mettler Toledo. The sample was heated from 25 to 120°C, kept at this temperature for 10 min and then cooled down again to 25°C. This temperature was kept again for 10 min and the cycle was repeated. The second cycle was used for the reported results. The heating rate was 10 K/min and the measurement was performed under a continuous flow of nitrogen (2 ml/min).

3.5 | Polarized optical microscopy

A small amount of the PF-initiator was placed on a glass slide. For temperature-dependent observations, the glass slide was placed on a LINKAM THMS 600 hot stage and the temperature adjusted. The sample was first melted at 120°C, kept at this temperature for 10 min and then cooled down to 30°C. After a further delay of 10 min, the sample was heated to 110°C. The sample was observed using an Axioplan 2 microscope from Carl Zeiss, Jena, Germany. The polarized optical microscopy (POM) images were recorded by an AxioCam MRC camera.

3.6 | Transmission electron microscopy

The blotting samples for TEM were prepared without any staining by transferring 3 µl of the block copolymer (20 µM) dissolved in water to a copper grid (Plano, Wetzlar, Germany) coated with Formvar film. After a waiting period of 1 min, the excess liquid was removed with filter paper. In the second process, 3 µl of an aqueous polymer solution (1 µM) was placed on the grid and the solvent evaporated at room temperature. The samples were studied with a Zeiss EM 900 transmission electron microscope (Carl Zeiss Microscopy GmbH, Oberkochen,

Germany). The images were taken with a SSCCD SM-1 K-120 camera (TRS, Moorenweis, Germany).

3.7 | X-ray scattering of the PF-initiator and the block copolymer powder

A Bruker D4 Endeavor (Bruker, Karlsruhe, Germany) diffractometer was used for wide-angle X-ray scattering (WAXS) measurements at room temperature with Cu K α radiation. The block copolymer powder was placed in a sample holder and fixed with a polyimide foil. The PF-initiator was dissolved in chloroform that was deposited on a silicon zero background substrate. The solvent was allowed to evaporate and a thin film is formed. All measurements were taken in a scan range of $2^\circ \leq 2\theta \leq 80^\circ$, with a step width of 0.01° and a recording time per step of 2 s. A separate background measurement was subtracted from the data.

4 | SYNTHESSES

4.1 | Macroinitiator with perfluorinated segment (PF-initiator)

1*H*,1*H*,12*H*,12*H*-Perfluoro-1,12-dodecanediol (PF-diol) (10 g, 17.8 mmol) and triethylamine (12.3 ml, 88.9 mmol) were dissolved in 100 ml freshly distilled THF in a one-neck-round bottom flask. The THF solution was cooled in ice/water bath. Subsequently, 2-bromoisobutryl bromide (16.7 ml, 71.16 mmol), diluted with 10 ml THF, was added dropwise using a dropping funnel under continuous stirring. The reaction was allowed to continue for 24 h. After filtration, THF was evaporated by rotary evaporator and the brownish crude product was dissolved in diethyl ether and washed with water, 0.1 N HCl, and 0.1 N NaOH until the aqueous phase had a neutral pH-value, followed by washing with brine. The organic phase was dried over sodium sulfate and filtered. Diethyl ether was removed by rotary evaporator and the product was recrystallized from *n*-hexane overnight at 4°C. The light yellow crystals were dissolved in toluene and eluted through a silica column with an excess of toluene. The resulting yellowish solution was concentrated and filtered. Toluene was completely evaporated by rotary evaporator and the solid product was recrystallized from *n*-hexane. The obtained white crystals were washed with cold *n*-hexane and dried under vacuum at room temperature. Yield: 6.2 g (40%).

^1H (500 MHz, CDCl_3): δ 1.96 (s, 12 H, $-\text{CH}_3$), 4.68 (t, $^3J[\text{F},\text{H}] = 13.1$ Hz, 4 H, $-\text{CH}_2$).

^{13}C (125 MHz, CDCl_3): δ 30.4 (s $-\text{[CH}_3\text{]}_2$), 53.9 (s $-\text{C}[\text{Br}]$), 60.7 (t, $-\text{CF}_2-\text{CH}_2-$, 2J 27.7 Hz), 110–116

($-\text{CF}_2-$), 170.3 (s, $-\text{O}-\text{C}[\text{O}]$), ^{19}F (470 MHz, CDCl_3): δ -123.27 (4 F, $-\text{CH}_2-\text{CF}_2-\text{CF}_2-$), -121.85 (12 F, $-\text{CF}_2-$), -119.42 (4 F, $^3J[\text{F},\text{H}] = 13.1$ Hz, $-\text{CH}_2\text{CF}_2-$) (^{13}C NMR spectrum is given in the Supporting Information S5.)

4.2 | Synthesis of alkyne-terminated monofunctional PPO

PPO monobutyl ether (PPO, 1000 g/mol) (10 g, 10 mmol), 5-hexynoic acid (1.23 g, 1.214 ml, 110 mmol), and DMAP (0.1833 g, 1.5 mmol) were dissolved in dry DCM (90 ml) in a round bottom flask. The solution was cooled in ice/water bath and then N,N' -diisopropyl carbodiimide (DIC) (1.8930 g, 2.323 ml, 0.015 mol) solution in dry DCM (10 ml) was added dropwise using a dropping funnel under continuous stirring. The reaction was allowed to continue for 24 h at room temperature and followed by filtration to remove the precipitate. The filtrate was washed two times with brine. The organic phase was dried over sodium sulfate and after filtration, the solvent was removed by rotary evaporator. The crude product was further purified by column chromatography (silica column, the polarity of mobile phase was varied from nonpolar to polar as: (a) *n*-hexane, (b) *n*-hexane/ethyl acetate 10:1 (vol/vol), (c) 5:3 (vol/vol), and (d) ethyl acetate). A yellowish and highly viscous product was recovered after solvent evaporation. Discoloration was achieved after passing the *n*-hexane solution of the product through alumina (neutral) column. The solution was concentrated by a rotary evaporator, filtered through a 0.2 μm PTFE syringe filter, and finally, the product was recovered after *n*-hexane evaporation under a stream of nitrogen for 3 days. Yield: 4.1 g (38%) The ^1H NMR spectrum is given in the Supporting Information S6.

4.3 | Synthesis of Br-PSMA-*b*-PF-*b*-PSMA-Br triblock copolymers by ATRP

In a typical reaction, copper(I) bromide (0.3069 g, 0.1392 mmol), 2,2'-bipyridine (bpy) (0.6682 g, 4.2784 mmol), and the bifunctional PF-initiator (0.6682 g, 4.2782 mmol) were transferred to a Schlenk tube (250 ml) which was then sealed with a rubber septum. The Schlenk tube was subjected to vacuum and then backfilling with nitrogen three times. The solution of SMA (50 ml, 51.4 g, 256.7 mmol) in dry acetonitrile (50 ml) was added to the Schlenk tube. The solution turned brown immediately indicating the formation of the Cu/byp complex. Byp created a stable and homogeneous copper complex with a good activation rate. It was frozen directly in liquid nitrogen and subjected to

five freeze-pump-thaw cycles for removal of oxygen from the reaction mixture. The Schlenk tube was then placed into an oil bath preheated to 40°C and the reaction continued for 36 min. The reaction was stopped by exposing the reaction content to air and adding to cold *n*-hexane. The color changed from brown to green indicating the oxidation of Cu(I) to Cu(II). The block copolymer formed a separate layer at the bottom, *n*-hexane was decanted and the copolymer was dissolved in THF and passed through alumina (neutral) column for the removal of copper. The solution was filtered after evaporating most of the THF by rotary evaporator. The Br-PSMA-*b*-PF-*b*-PSMA-Br copolymer was recovered as a white powder after precipitation at least three times in cold *n*-hexane and drying under a stream of nitrogen at room temperature. To remove all monomers precipitation was repeated three times. The white polymer was dried in vacuum and under nitrogen flow at room temperature. Yield: 7.4 g (conversion 40%), calculated degree of polymerization of PSMA: 96, (Br-PSMA₄₈-*b*-PF-*b*-PSMA₄₈-Br).

^1H (500 MHz, $\text{DMSO}-d_6$): δ 0.86 (m, 0.64–1.06 ppm, $-\text{C}(-\text{CH}_3)-\text{C}(=\text{O})-\text{O}-$), 1.32 (m, 1.18–1.41 ppm, $[\text{CH}_3]_2-\text{C}-$), 1.81 (m, 1.60–2.06 ppm, $-\text{CH}_2-\text{C}(-\text{CH}_3)-$), 3.69 (m, 3.59–3.78 ppm, $-\text{O}-\text{CH}_2-\text{CH}-[-\text{O}]-\text{CH}_2$), 3.92 (m, 3.79–3.99 ppm, $-\text{O}-\text{CH}_2-\text{CH}(-\text{O})-\text{CH}_2-\text{O}-\text{C}(=\text{O})-$), 4.00 (m, 3.99–4.08 ppm, $-\text{O}-\text{CH}_2-\text{CH}(-\text{O})-\text{CH}_2-\text{O}-\text{C}(=\text{O})-$), 4.27 (m, 4.20–4.35 ppm, $-\text{O}-\text{CH}_2-\text{CH}(-\text{O})-\text{CH}_2-\text{O}-\text{C}(=\text{O})-$). ^{19}F (470 MHz, $\text{DMSO}-d_6$): δ -122.78 (m, -123.20 to 124.40 ppm) $-\text{CH}_2-\text{CF}_2-\text{CF}_2-$), -121.59 (m, -122.16 to 121.04, $-\text{CF}_2-$), -118.38 (m, -118.73 to 117.97, $-\text{CH}_2\text{CF}_2-$). (^1H and ^{19}F NMR spectra are given in the Supporting Information S7).

4.4 | Synthesis of PPO-*b*-PSMA-*b*-PF-*b*-PSMA-*b*-PPO pentablock copolymers

For this purpose, the formed Br-PSMA-*b*-PF-*b*-PSMA-Br was transformed into N_3 -PSMA-*b*-PF-*b*-PSMA- N_3 by treatment with NaN_3 . The reaction conditions and characterization are described in Supporting Information (S8). The synthesis of PPO-*b*-PSMA-*b*-PF-*b*-PSMA-*b*-PPO was achieved via CuAAC reaction between alkyne-terminated PPO and N_3 -PSMA-*b*-PF-*b*-PSMA- N_3 . As an example, a Schlenk tube (250 ml), with a magnetic stirrer bar, was charged with N_3 -PSMA₁₉-*b*-PF-*b*-PSMA₁₉- N_3 (2 g, 0.2247 mmol), alkyne-terminated PPO (0.7376 g, 0.6742 mmol), and CuBr (0.0322 g, 0.2247 mmol) and closed by a rubber septum. Oxygen from the Schlenk tube was removed by several vacuum-nitrogen cycles, followed by the addition of dry THF (20 ml) and dry TEA (60 ml). The reaction solution was bubbled slowly with nitrogen for approximately 1 h. Meanwhile, the solution

color changed from green to brown. The reaction was carried out at 60°C for 3 days. The solvent and unreacted TEA were removed by rotary evaporator and the product was dissolved in THF and eluted through an alumina (neutral) column to remove copper, recovered by precipitation in cold *n*-hexane and drying under a stream of nitrogen at room temperature. Yield: 1.2 g (49%).

^1H (500 MHz, DMSO-*d*₆): δ 0.87 (m, 0.66–0.99 ppm, $-\text{C}(\text{CH}_3)_2-\text{C}(=\text{O})-\text{O}-$), 1.02 (m, 0.99–1.09 ppm, $-\text{CH}_2-\text{CH}(\text{CH}_3)-$), 1.31 (m, 1.17–1.40 ppm, $[\text{CH}_3]_2-\text{C}-$), 1.79 (m, 1.58–2.09 ppm, $-\text{CH}_2-\text{C}[\text{CH}_3]-$), 3.39 (m, 3.15–3.56 ppm, $-\text{CH}_2-\text{CH}[\text{CH}_3]-$), 3.68 (m, 3.56–3.77 ppm, $-\text{O}-\text{CH}_2-\text{CH}(\text{O})-\text{CH}_2-\text{O}-\text{C}(=\text{O})-$), 3.90 (m, 3.77–3.96 ppm, $-\text{O}-\text{CH}_2-\text{CH}(\text{O})-\text{CH}_2-\text{O}-\text{C}(=\text{O})-$), 4.01 (m, 3.96–4.09 ppm, $-\text{O}-\text{CH}_2-\text{CH}(\text{O})-\text{CH}_2-\text{O}-\text{C}(=\text{O})-$), 4.25 (m, 4.17–4.34 ppm, $-\text{O}-\text{CH}_2-\text{CH}(\text{O})-\text{CH}_2-\text{O}-\text{C}(=\text{O})-$). ^{19}F (470 MHz, DMSO-*d*₆): δ -122.79 (m, -123.33 to 124.50 ppm, $-\text{CH}_2-\text{CF}_2-\text{CF}_2-$), -121.59 (m, -122.16 to 121.07, $-\text{CF}_2-$), -118.39 (m, -118.82 to 118.02, $-\text{CH}_2\text{CF}_2-$).

4.5 | Synthesis of triphilic PPO-*b*-PGMA-*b*-PF-*b*-PGMA-*b*-PPO pentablock copolymers

In a typical reaction, PPO₁₅-*b*-PSMA₁₉-*b*-PF-*b*-PSMA₁₉-*b*-PPO₁₅ (0.8 g, 0.072 mmol) was dissolved in 1,4-dioxane (40 ml) in a 100 ml one-neck round bottom flask equipped with a magnetic stirrer bar and drying tube. Subsequently, 1 N HCl (4 ml) was added dropwise. The reaction continued for 2 days at room temperature under continuous stirring during which the solution turned turbid. The reaction mixture was neutralized by adding 1 M NaOH solution. The solvent was removed by rotary evaporator and the product was dispersed in methanol, filtered through a filter paper, and passed through an alumina (neutral) column. The solution was concentrated by a rotary evaporator, filtered through a 0.2 μm pore size filter, precipitated in cold diethyl ether. For final purification, the polymers were dissolved in water, added to the Amicon Ultra-15 dialysis system (Ultracel - 3 K, Merck, Germany, regenerated cellulose, pore size 3000 Da) and centrifuged for 20 min at 4000 rpm (Centrifuge 5810R, Eppendorf, 50,389 Wesseling-Berzdorf, Germany). The supernatant was diluted with deionized water and centrifuged again. This process was performed three times. Finally, the product, PPO₁₅-*b*-PGMA₄₈-*b*-PF-*b*-PGMA₄₈-*b*-PPO₁₅ was recovered after dissolving in water and freeze-drying. Yield: (0.063 g, 10%).

^1H (500 MHz, DMSO-*d*₆): δ 0.91 (m, 0.38–1.08 ppm, $-\text{CH}_2-\text{C}(\text{CH}_3)_2-$), 1.03 (m, 1.01–1.07 ppm, $\text{O}-\text{CH}_2-\text{CH}(\text{CH}_3)-$), 1.73 (m, 1.54–2.24 ppm, $-\text{CH}_2-\text{C}$

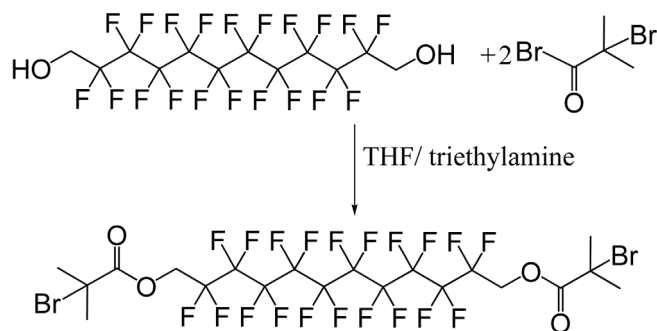
$(-\text{CH}_3)-$), 3.34 (m, 3.12–3.56 ppm, $-\text{O}-\text{CH}_2-\text{CH}(\text{CH}_3)-$), $-\text{O}-\text{CH}_2-\text{CH}(\text{O})-\text{CH}_2-\text{O}-\text{C}(=\text{O})-$), 3.70 (m, 3.61–3.82 ppm, $-\text{O}-\text{CH}_2-\text{CH}(\text{O})-\text{CH}_2-\text{O}-\text{C}(=\text{O})-$), 3.89 (m, 3.82–4.09 ppm, $-\text{C}(=\text{O})-\text{O}-\text{CH}_2-\text{CH}-$), 4.98 (m, 4.70–5.48 ppm, $\text{HO}-\text{CH}_2-\text{O}-$) ^{19}F (470 MHz, DMSO-*d*₆): δ -122.90 (m, -123.10 to 122.59 ppm, $-\text{CH}_2-\text{CF}_2-\text{CF}_2-$), -121.65 (m, -121.99 to 121.31, $-\text{CF}_2-$), -118.46 (m, -118.70 to 118.27, $-\text{CH}_2\text{CF}_2-$). (^1H NMR spectrum is given in the Supporting Information S9).

5 | RESULTS AND DISCUSSION

Well-defined triphilic pentablock copolymers, poly(propylene oxide)-*b*-poly(glycerol methacrylate)-*b*-perfluorinated segment-*b*-poly(glycerol methacrylate)-*b*-poly(propylene oxide), PPO-*b*-PGMA-*b*-PF-*b*-PGMA-*b*-PPO of various compositions have been synthesized by a combined approach of ATRP and Cu(I) catalyzed azide-alkyne CuAAC reaction.

5.1 | Characterization of the macroinitiator with perfluorinated segment (PF-initiator)

In the first step, 1H,1H,12H,12H-perfluoro-1,12-dodecanediol (PF-diol) was transformed into bifunctional ATRP initiator (PF-initiator) by reacting with α -bromoisobutyryl bromide in THF in the presence of triethylamine at 0°C as outlined in Scheme 1. Figure 1(A) depicts the ^1H NMR spectrum of the PF-initiator, where the presence of signal *a* ($\delta \sim 1.96$ ppm) from the methyl protons of the isobutyryl moiety confirms the synthesis of the initiator. The signal *b* ($\delta \sim 4.68$ ppm) corresponds to the methylene protons next to the perfluorinated segment. Comparison of the integrals of these two peaks suggests 100% esterification of the hydroxyl groups of the PF-diol.



SCHEME 1 Synthesis of the PF-initiator. PF, perfluoroalkyl

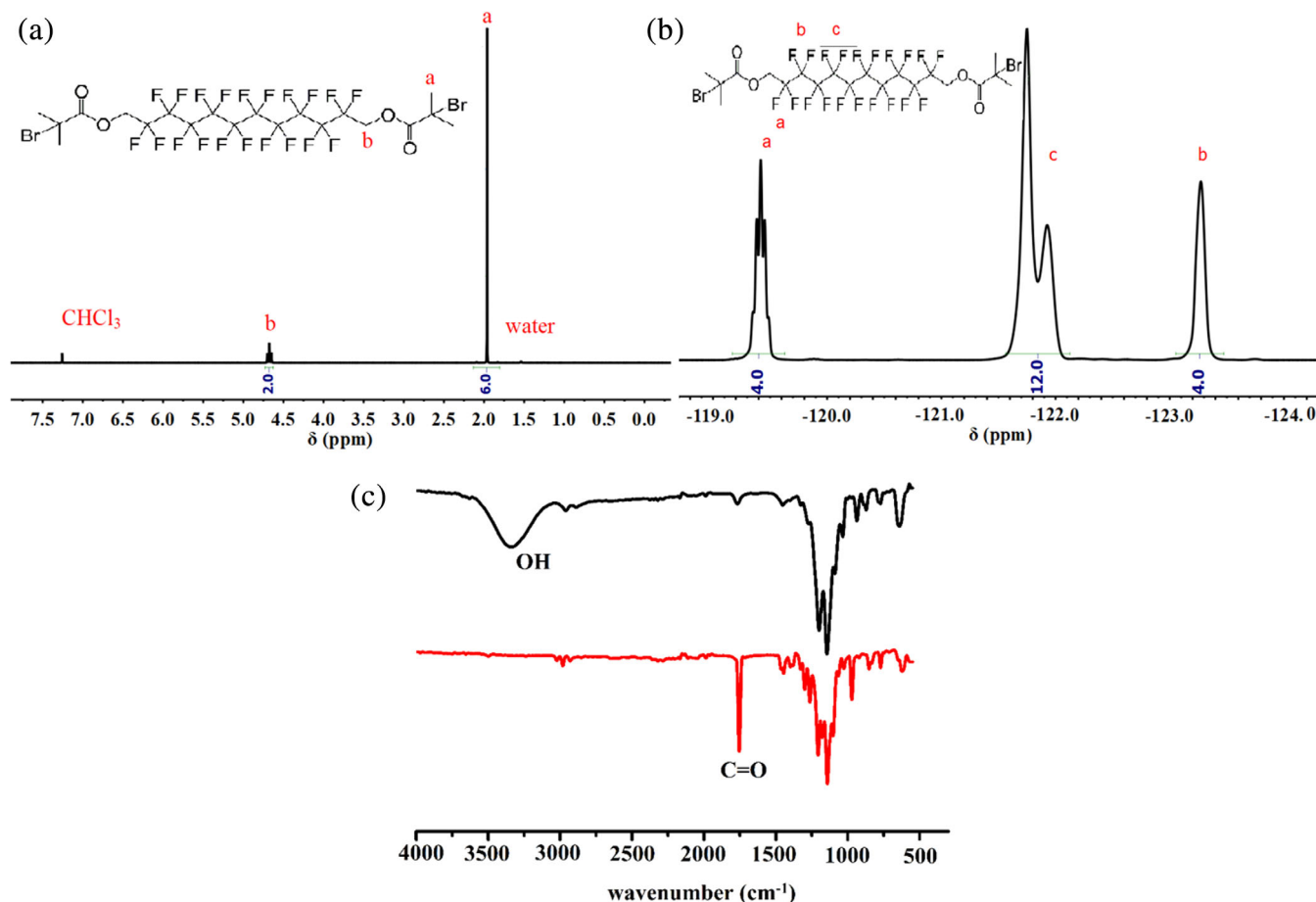


FIGURE 1 Spectra of PF-initiator (A) ^1H NMR (500 MHz, CDCl_3), (B) ^{19}F NMR (470 MHz, CDCl_3), and (C) FTIR spectra of PF-diol (top) and PF-initiator (bottom). FTIR, Fourier transform infrared; PF, perfluoroalkyl; PGMA, poly(glycerol monomethacrylate); PPO, poly(propylene oxide) [Color figure can be viewed at wileyonlinelibrary.com]

The splitting of signal *b* into a triplet is due to the 3 *J* coupling of CH_2 with CF_2 .³⁷ In the ^{19}F NMR spectrum (Figure 1(B)) the signal *a* at $\delta \approx -119$ ppm arises from the CF_2 next to CH_2 ($-\text{CH}_2-\text{CF}_2-$, triplet), while the peak *b* at $\delta \approx -123$ ppm can be assigned to the second CF_2 group and the other CF_2 fluorine atoms appear at $\delta \approx -121$ ppm (peak *c*).³⁸ The APT ^{13}C NMR spectrum of the initiator is provided in Supporting Information S5.

Further evidence of the successful synthesis came from the FTIR spectra as depicted in Figure 1(C), where the peak at the wavenumber $\nu = 3325 \text{ cm}^{-1}$ that corresponds to the OH-group of the PF-diol completely disappeared after reaction with α -bromoisobutyryl bromide and a characteristic peak of the $\text{C}=\text{O}$ stretching vibration of the ester bond system appeared at $\nu = 1755 \text{ cm}^{-1}$. To test the stability of the formed initiator against acid hydrolysis, the PF-initiator was treated under weakly acidic conditions for 48 h and was found to be stable against acid hydrolysis of the ester bond. The stability can be attributed to the CH_2 spacer between the ester bond system and the CF_2 groups of the initiator.³⁹ (^1H

NMR spectra are provided in Supporting Information S10.)

5.2 | Solid–solid phase transition of the PF-initiator

The DSC heating trace of the PF-initiator (Figure 2(A)) exhibits two endothermic phase transitions, one with the peak maximum at 63°C , ($\Delta H = 8.6 \text{ kJ/mol}$) and the second more prominent one at 95°C , ($\Delta H = 24.8 \text{ kJ/mol}$). The cooling trace from the isotropic melt reveals two exothermic phase transitions at 82 and 42°C . The PF-diol is a highly crystalline material with $T_m = 166^\circ\text{C}$ (the DSC plot is given in the Supporting Information S11) and it can be argued that after converting PF-diol into PF-initiator, the interaction between the OH-groups and the dipole–dipole interactions of the perfluorinated chains are weakened, which might result in the decrease of the melting temperature from 166°C for the PF-diol to 95°C for the PF-initiator.⁴⁰ Regarding the phase transition at

63°C prior to crystal melting, the formation of a liquid crystalline phase can be excluded as the relationship between the melting enthalpy and the so-called clearing enthalpy of a liquid crystalline phase would be inverse.^{41–43} There are known pretransitions or solid–solid phase transitions in semifluorinated alcohols and perfluoro-*n*-alkanoic acids, for example, F₆H₁₁OH and F₁₁COOH.^{44–46} To visualize the solid–solid phase transition of the PF-initiator, POM images were acquired at 30, 70, and 110°C during the heating cycle and are included as insets in Figure 2(A). It is evident that the morphology and the chromaticity of the crystals change with phase transitions and after melting an isotropic liquid is formed. To get further insight, temperature-dependent WAXS studies were carried out.

Temperature-dependent WAXS traces of PF-initiator powder confirm the DSC observations (see Supporting Information S12). During heating, some Bragg reflections disappear above 60°C and a new peak at 15° appears, which could be attributed to the solid–solid phase transition as also observed in DSC thermograms before the crystal melting and which is known for PTFE.⁴⁷

The formation of a crystalline lamellar structure is evident after drying chloroform solution of the PF-initiator and thin film formation as depicted in Figure 2 (B). In the full range of observation, reflections up to the 19th order can be observed, leading to a lamellar thickness of 23.75 Å. The peaks above fifth order are overlapping with the WAXS signals, especially the high-intense 10th-order peak at $2\theta = 38^\circ$ is at the same position as a WAXS reflection. Therefore, a reconstruction of the electron density distribution is not reliable. Nevertheless, the obtained thickness is in good agreement with the dimension of the initiator molecule shown in Scheme 1.

5.3 | Synthesis and characterization of triphilic PPO-*b*-PGMA-*b*-PF-*b*-PGMA-*b*-PPO pentablock copolymers

By employing the PF-initiator, in a first step well-defined Br-PSMA-*b*-PF-*b*-PSMA-Br triblock copolymers were synthesized by ATRP of SMA at 40°C in acetonitrile, using Cu(I)Br/2,2'-bipyridine as a catalyst system (Scheme 2).

Two Br-PSMA_{*x*}-*b*-PF-*b*-PSMA_{*x*}-Br triblock copolymers with *x* = 19 or 48 were prepared (see Table 1 for details). To preserve the maximum chain-end bromine functionality, the polymerization was stopped at a relatively low monomer conversion of ≤40%.^{48,49} Figure 3(A) shows the ¹H NMR spectrum of the Br-PSMA₄₈-*b*-PF-*b*-PSMA₄₈-Br triblock copolymer. The peaks observed in the spectrum are well correlated to the protons of the PSMA blocks. Furthermore, the signals of the fluorinated block could also be observed in the respective ¹⁹F NMR spectrum. The degree of polymerization of the PSMA segment was estimated by combining ¹⁹F NMR and ¹H NMR spectroscopy (see Supporting Information S13 for details) and the data are tabulated in Table 1.

Kinetic studies of ATRP of SMA with PF-initiator were also carried out and the data are shown in Figure 4. The linear relationship of $\ln([M_0]/[M_t])$ with $[M_0]$ the initial monomer concentration and $[M_t]$ the monomer concentration at a given time *t* versus reaction time (Figure 4 (A)) shows that the polymerization is of first-order with respect to monomer concentration and that the concentration of growing active radicals remains constant throughout the reaction. However, a slight deviation from linearity could be seen at longer reaction times (*t* = 240 min) indicating the formation of some dead polymer chains (irreversibly terminated) at higher conversion. The highly controlled nature of the polymerization

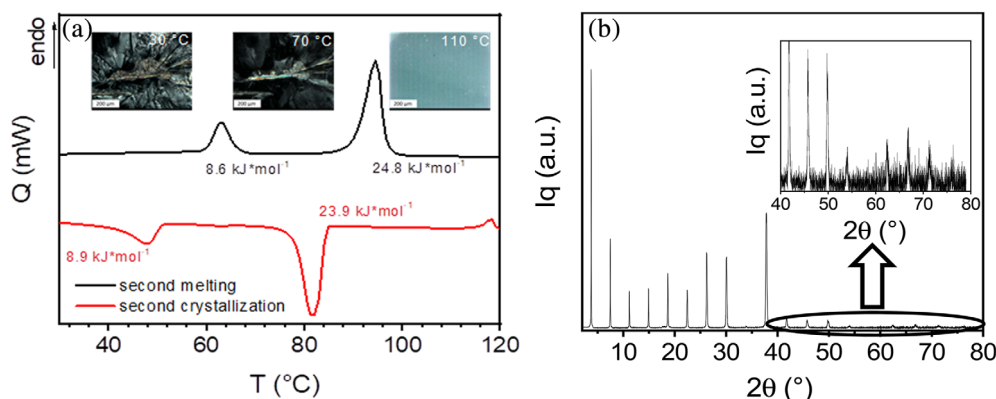
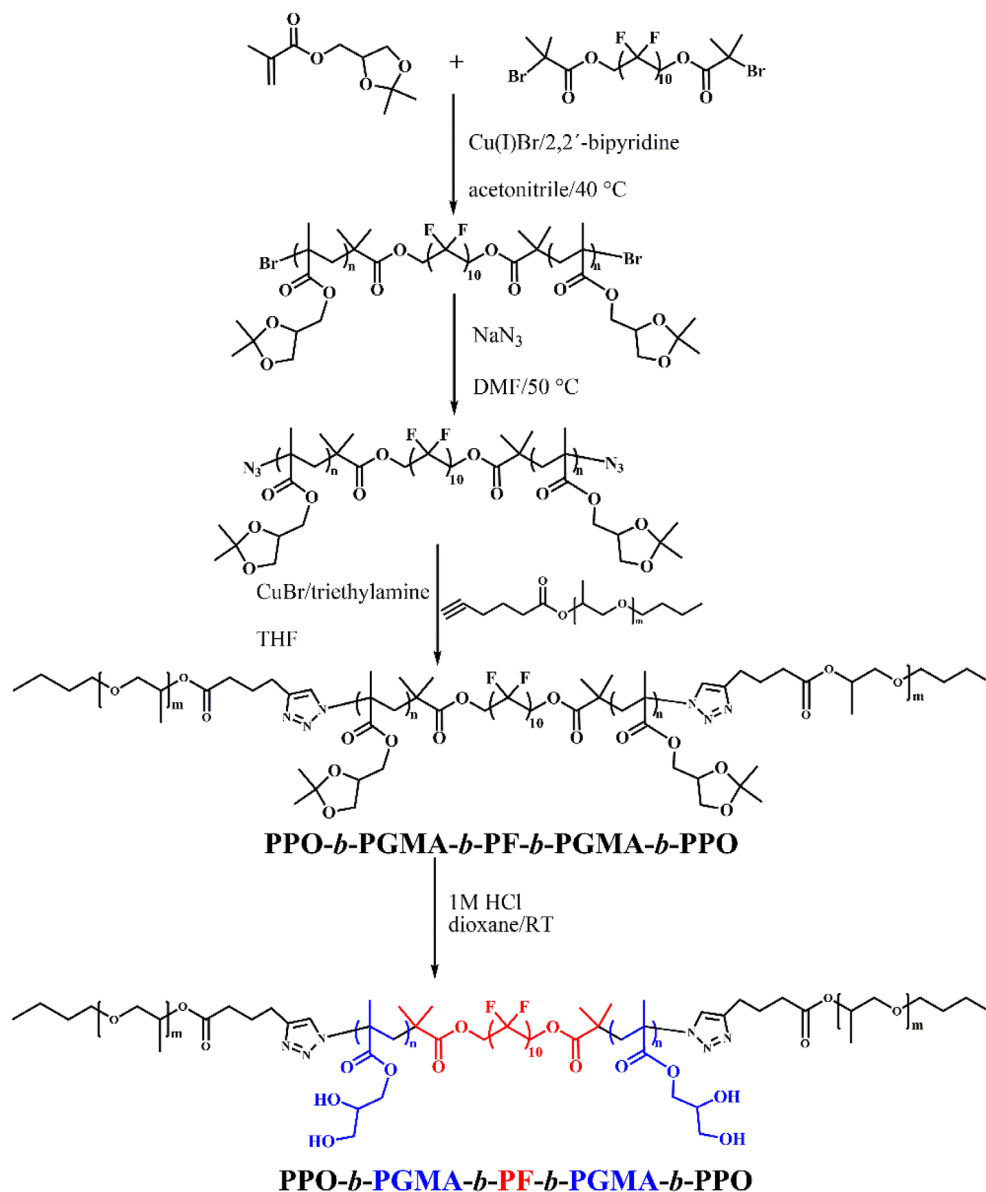


FIGURE 2 (A) DSC heating and cooling traces of the PF-initiator at heating/cooling rates of 10 K/min. As inset, polarized optical microscopy images of the PF-initiator at three temperatures are given. (B) WAXS diffractogram (*I*-*q* vs. 2θ) at room temperature of PF-initiator film prepared from chloroform solution. The inset shows enlarged the peaks from 11th to 19th order. DSC, differential scanning calorimetry; PF, perfluoroalkyl; WAXS, wide-angle X-ray scattering [Color figure can be viewed at wileyonlinelibrary.com]

SCHEME 2 Synthesis of triphilic PPO-*b*-PGMA-*b*-PF-*b*-PGMA-*b*-PPO pentablock copolymers. PF, perfluoroalkyl; PGMA, poly(glycerol monomethacrylate); PPO, poly(propylene oxide) [Color figure can be viewed at wileyonlinelibrary.com]



is also evident from the monomodal progression of GPC traces (Figure 4(C)), low-polydispersity indices throughout the polymerization reaction (in the range of $PDI \approx 1.2$) (Figure 4(B)), and linear increase of M_n as a function of monomer conversion (Figure 4(D)).

The experimentally determined M_n values for the polymerization of SMA using the PF initiator by ATRP are comparable with the predicted M_n values (Figure 4(D)).

PPO-*b*-PSMA-*b*-PF-*b*-PSMA-*b*-PPO pentablock copolymers were achieved from Br-PSMA-*b*-PF-*b*-PSMA-Br and PPO via CuAAC chemistry. First, the terminal bromine of Br-PSMA-*b*-PF-*b*-PSMA-Br was substituted with azide by reacting with NaN_3 in DMF at 50 °C. The formation of N_3 -PSMA-*b*-PF-*b*-PSMA- N_3 was confirmed by Fourier transform infrared (FTIR) spectra shown in Supporting Information S8. Separately, PPO was coupled with 5-hexynoic acid that afforded alkyne-terminated

PPO. Subsequently, the CuAAC reaction between N_3 -PSMA-*b*-PF-*b*-PSMA- N_3 and alkyne-terminated PPO afforded PPO-*b*-PSMA-*b*-PF-*b*-PSMA-*b*-PPO pentablock copolymers (Scheme 2). Figure 3(B) depicts the typical ^1H NMR spectrum of PPO-*b*-PSMA-*b*-PF-*b*-PSMA-*b*-PPO with peak assignment and chemical structure, where in addition to the PSMA signals, the signals of PPO (g, h, and i) could also be seen (detailed ^1H NMR spectrum is given in Supporting Information S14). The reaction was also confirmed by the complete disappearance of azide signals in the FTIR spectrum after the CuAAC reaction (the FTIR spectrum is given in Supporting Information S15). Further evidence for successful synthesis came from the GPC traces shown in Figure 5 that reveal a significant peak shift toward higher molar mass that is, lower retention times after the CuAAC reaction with no traces of unreacted PPO.

TABLE 1 Characterization of the synthesized block copolymers

Sample	$M_n(1H\ NMR)^a$ (g/Mol)	$M_n(GPC)$ (g/Mol)	PDI
PPO ₁₅ - <i>b</i> -PSMA ₁₉ - <i>b</i> -PF- <i>b</i> -PSMA ₁₉ - <i>b</i> -PPO ₁₅	10,500	12,400	1.13
PPO ₄₂ - <i>b</i> -PSMA ₁₉ - <i>b</i> -PF- <i>b</i> -PSMA ₁₉ - <i>b</i> -PPO ₄₂	13,600	15,100	1.26
PPO ₁₅ - <i>b</i> -PSMA ₄₈ - <i>b</i> -PF- <i>b</i> -PSMA ₄₈ - <i>b</i> -PPO ₁₅	22,100	20,800	1.10
PPO ₄₂ - <i>b</i> -PSMA ₄₈ - <i>b</i> -PF- <i>b</i> -PSMA ₄₈ - <i>b</i> -PPO ₄₂	25,200	23,900	1.17
PPO ₁₅ - <i>b</i> -PGMA ₁₉ - <i>b</i> -PF- <i>b</i> -PSMA ₁₉ - <i>b</i> -PPO ₁₅	9500	17,700	1.20
PPO ₄₂ - <i>b</i> -PGMA ₁₉ - <i>b</i> -PF- <i>b</i> -PGMA ₁₉ - <i>b</i> -PPO ₄₂	12,700	14,600	1.14
PPO ₁₅ - <i>b</i> -PGMA ₄₈ - <i>b</i> -PF- <i>b</i> -PGMA ₄₈ - <i>b</i> -PPO ₁₅	19,700	37,200	1.10
PPO ₄₂ - <i>b</i> -PGMA ₄₈ - <i>b</i> -PF- <i>b</i> -PGMA ₄₈ - <i>b</i> -PPO ₄₂	22,800	23,600	1.10
Br-PGMA ₁₉ - <i>b</i> -PF- <i>b</i> -PGMA ₁₉ -Br	7400	17,400	1.19
Br-PGMA ₄₈ - <i>b</i> -PF- <i>b</i> -PGMA ₄₈ -Br	17,500	34,100	1.10

Abbreviations: GPC, gel permeation chromatography; PF, perfluoroalkyl; PGMA, poly(glycerol monomethacrylate); PPO, poly(propylene oxide).

^a $M_n = M_n$ of PSMA/PGMA (the degree of polymerization M_n of PSMA and hence PGMA were calculated from ¹⁹F NMR to ¹H NMR spectra, (see Supporting information S12 for details) + 2 M_n of PPO_{15/42} + molar mass of the initiator.

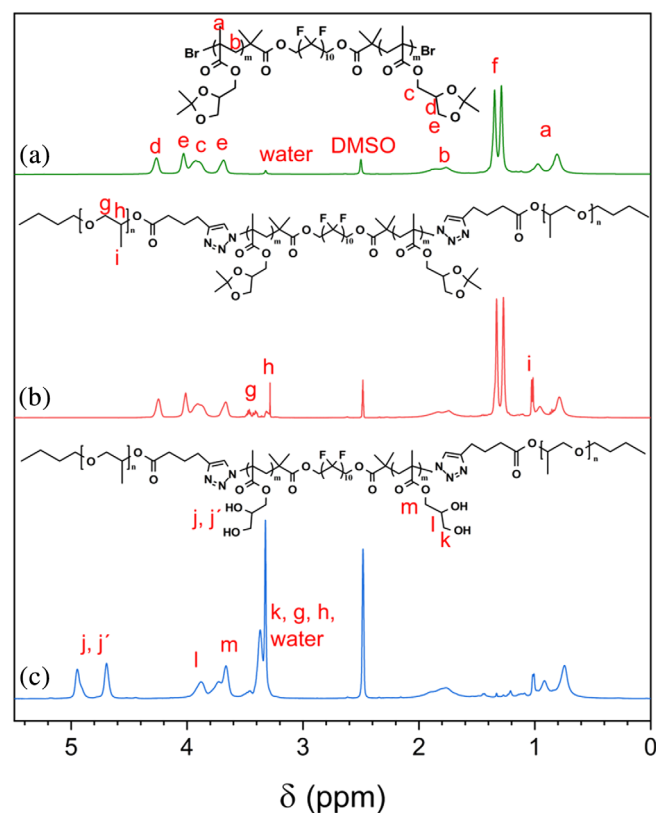


FIGURE 3 ¹H NMR spectra (500 MHz, DMSO-*d*₆) of (a) Br-PSMA₄₈-*b*-PF-*b*-PSMA₄₈-Br, (b) PPO₁₅-*b*-PSMA₄₈-*b*-PF-*b*-PSMA₄₈-*b*-PPO₁₅, and (c) PPO₁₅-*b*-PGMA₄₈-*b*-PF-*b*-PGMA₄₈-*b*-PPO₁₅. PF, perfluoroalkyl; PGMA, poly(glycerol monomethacrylate); PPO, poly(propylene oxide) [Color figure can be viewed at wileyonlinelibrary.com]

Finally, the acid hydrolysis of the acetonide moiety of PSMA segments of PPO-*b*-PSMA-*b*-PF-*b*-PSMA-*b*-PPO with HCl generated water soluble triphilic pentablock

copolymers, PPO-*b*-PGMA-*b*-PF-*b*-PGMA-*b*-PPO (Scheme 2). The ¹H NMR spectrum after hydrolysis (Figure 3(C)) reveals the complete disappearance of the signals of methyl protons of the acetonide ring (denoted as *f* in Figure 3(B)) and the appearance of OH signals (*j* and *j'*). The GPC trace (Figure 5) shifts toward lower elution time with a monomodal molar mass distribution and narrow polydispersity indices after the acid hydrolysis (Table 1). Both the ¹H NMR and GPC data provide a clear evidence for the formation of well-defined PPO-*b*-PGMA-*b*-PF-*b*-PGMA-*b*-PPO pentablock copolymers. An obvious discrepancy exists between the molar masses of PPO₁₅-*b*-PSMA₄₈-*b*-PF-*b*-PSMA₄₈-*b*-PPO₁₅ and PPO₁₅-*b*-PGMA₄₈-*b*-PF-*b*-PGMA₄₈-*b*-PPO₁₅. Basically the deprotection of the PSMA block to the PGMA block by the formation of acetone as low molar mass by-product should lead to a pentablock copolymer with PGMA blocks having a slightly lower mass than the respective block copolymer with PSMA blocks. But as shown in Table 1 the molar mass increases upon deprotection from 20,800 to 37,200 g/mol. This is an apparent increase of the molar mass also observed by GPC in DMF for other block copolymers upon PGMA deprotection.⁵⁰ A possible reason is that DMF is a better solvent for PGMA containing block copolymers compared with the respective species containing PSMA blocks. Thus, PGMA containing block copolymers occupy a larger hydrodynamic volume. The appearance of the high molar mass bump in PPO₁₅-*b*-PGMA₄₈-*b*-PF-*b*-PGMA₄₈-*b*-PPO₁₅ can also be explained by the amphiphilic nature of this block copolymer dissolved in DMF, which might lead to the formation of first small polymer aggregates. The synthesized pentablock copolymers are triphilic, that is, equipped with three immiscible segments of different philicities, namely, fluorophilic perfluorinated segment, hydrophilic PGMA, and lipophilic PPO blocks.

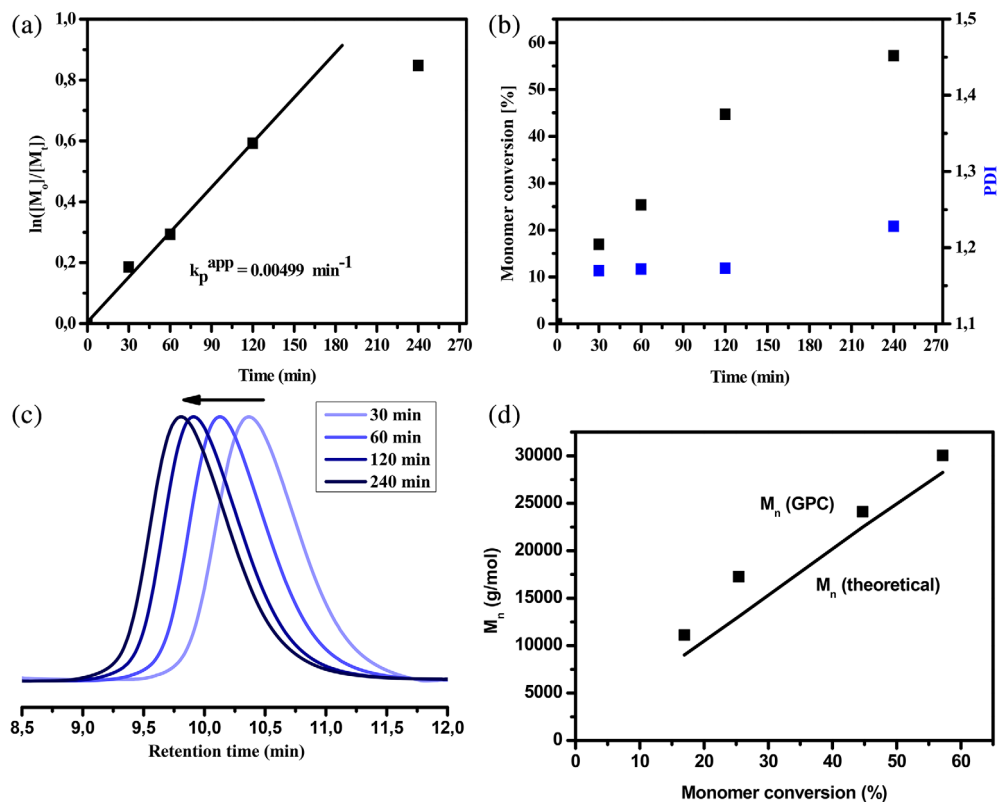


FIGURE 4 Kinetic data of the ATRP of solketal methacrylate using bifunctional perfluorinated initiator to yield the polymer Br-PSMA-*b*-PF-*b*-PSMA-Br. (A) First-order kinetic plot, (B) monomer conversion and polydispersity index as function of reaction time, (C) the respective GPC traces, and (D) evolution of molar mass (M_n , GPC) with monomer conversion. In M_n (theoretical, full line), the molar mass of the PF initiator (858 g/mol) is also included. Reaction conditions were as: 40°C, monomer:acetonitrile = 1:1 (vol/vol), [monomer]:[PF-initiator]:[Cu(I)Br]:[bpy] = 120:1:1:2. ATRP, atom transfer radical polymerization; GPC, gel permeation chromatography; PF, perfluoroalkyl [Color figure can be viewed at wileyonlinelibrary.com]

The schematic presentation and contour lengths of the fully extended segments of the formed pentablock copolymers are depicted in Scheme 3. The length of a GMA unit in a fully extended PGMA chain is $l_{\text{GMA}} = 0.255 \text{ nm}$ and for PPO the length of the repeat unit is $l_{\text{PPO}} = 0.36 \text{ nm}$.^{51,52} The 1,4-disubstituted triazole ring has a length of $\sim 0.5 \text{ nm}$.⁵³ BIOVIA Materials Studio calculated the length of the spacer between the triazole ring and the PPO block as 0.511 nm and that of the PF-initiator as 2.3 nm. The space-filling models of the PF-initiator and block copolymers are also included in Scheme 3.

To find out the nanophase separation and possible crystallization of the PF segment in block copolymers, WAXS studies were carried out. Figure 6 depicts a powder WAXS trace of the triphilic PPO₁₅-*b*-PGMA₄₈-*b*-PF-*b*-PGMA₄₈-*b*-PPO₁₅ pentablock copolymer. It is evident that the two signals of the amorphous PF-initiator observed at $2\theta \sim 18^\circ$ and weakly at 40° (Supporting Information S12) appear also in the block copolymer. Russel et al.⁵⁴ also observed a broadened peak at $2\theta \sim 18^\circ$ for perfluorinated segments when an alkyl sequence $(\text{CH}_2)_m$ with $m \geq 16$ was attached, which can be interpreted as an 2D-

pseudo-hexagonal mesomorphic phase.⁵⁵ As no melting peak in DSC measurements was found, it can be argued that the PF segments phase separate in block copolymer by forming not well-ordered, amorphous domains. This could be attributed to the fact that the PF segments after connecting to block copolymer chains at both ends lose their chain-end mobility that is required for placement of the chain in the regular crystal lattice. Additionally, the large space requirements of the adjacent PGMA blocks might contribute to the hindered crystallization of the central PF moiety (see Scheme 3 and Supporting Information S16). Amorphous PGMA shows also two halos, located at 18° and 30° ,⁵⁶ completing the observed signals in Figure 6.

5.4 | Morphology formation of triphilic PPO-*b*-PGMA-*b*-PF-*b*-PGMA-*b*-PPO pentablock copolymers

Amphiphilic block copolymers generally form self-assembled nanostructures composed of hydrophobic domains surrounded by hydrophilic segments in aqueous

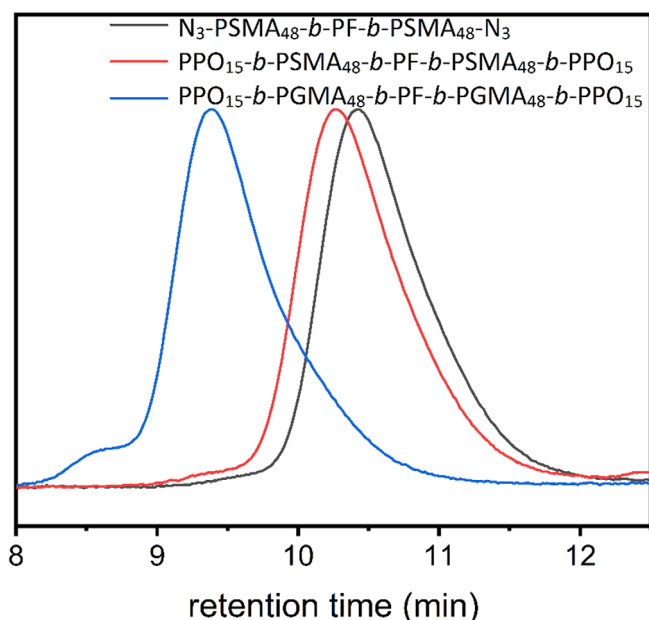
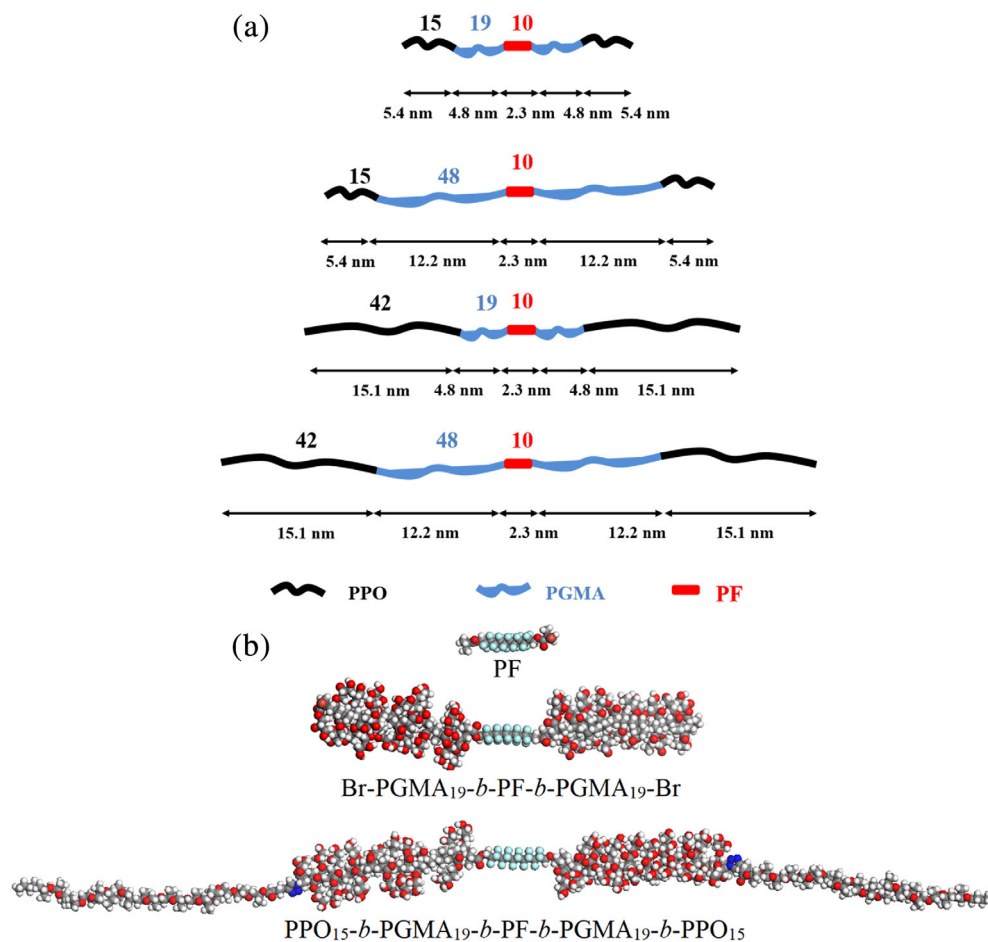


FIGURE 5 Gel permeation chromatography traces of N_3 -PSMA₄₈-*b*-PF-*b*-PSMA₄₈- N_3 , PPO₁₅-*b*-PSMA₄₈-*b*-PF-*b*-PSMA₄₈-*b*-PPO₁₅ and PPO₁₅-*b*-PGMA₄₈-*b*-PF-*b*-PGMA₄₈-*b*-PPO₁₅ in 10 mM (LiBr) DMF solution at 25°C. DMF, Dimethylformamide; PF, perfluoroalkyl; PGMA, poly(glycerol monomethacrylate); PPO, poly(propylene oxide) [Color figure can be viewed at wileyonlinelibrary.com]

solution. The triphilic block copolymers, due to immiscibility of its fluorophilic and lipophilic segments, could self-assemble into uniquely phase separated nanostructured hydrophobic domains with distinct fluorophilic and lipophilic compartments, depending upon chemistry, architecture, and composition.

A 20 μ M aqueous solution of PPO₁₅-*b*-PGMA₁₉-*b*-PF-*b*-PGMA₁₉-*b*-PPO₁₅ was deposited onto a copper grid coated with Formvar film and after waiting for 1 min, the excess solution was carefully removed with a filter paper. The TEM image of the phase-separated nanostructure is depicted in Figure 7(A) where spherical or slightly ellipsoidal structures in the range of \sim 200 nm in diameter can be seen. Each structure has several disordered dark domains (size \sim 17 nm) dispersed in the gray matrix. The dark areas in the TEM image represent regions with higher electron density. Thus, they can be assigned to PF-rich domains since they have the highest electron density among the three blocks in the copolymer under investigation.

However, because of the large sizes of these aggregates, it can be assumed that some of the fluorinated segments could also be dispersed in the gray areas. The gray matrix represents mostly the PPO segments. The morphology of the nanostructures transformed from spherical to filament-like structures when a different preparatory



SCHEME 3 (A) Schematic presentation of PPO-*b*-PGMA-*b*-PF-*b*-PGMA-*b*-PPO pentablock copolymers together with the calculated contour lengths of the fully extended chains of various compositions. (B) Space-filling model of the fluorinated initiator (top), the amphiphilic Br-PGMA₁₉-*b*-PF-*b*-PGMA₁₉-Br (middle) and the triphilic block copolymer PPO₁₅-*b*-PGMA₁₉-*b*-PF-*b*-PGMA₁₉-*b*-PPO₁₅ (bottom). PF, perfluoroalkyl; PGMA, poly(glycerol monomethacrylate); PPO, poly(propylene oxide) [Color figure can be viewed at wileyonlinelibrary.com]

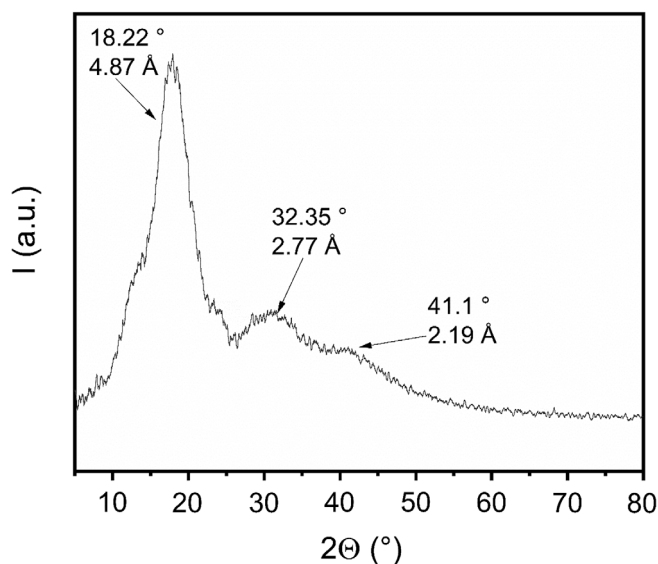


FIGURE 6 Wide-angle X-ray scattering diffractogram (powder) of PPO₁₅-*b*-PGMA₄₈-*b*-PF-*b*-PGMA₄₈-*b*-PPO₁₅ pentablock copolymer, showing amorphous signals of PTFE (~18° and 41°) and PGMA (~18° and 30°). PF, perfluoroalkyl; PGMA, poly(glycerol monomethacrylate); PPO, poly(propylene oxide)

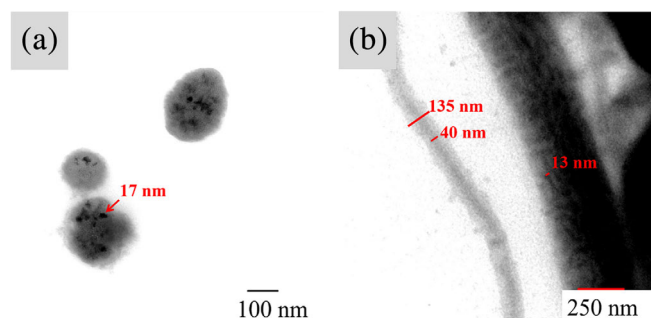


FIGURE 7 Transmission electron microscopy images of PPO₁₅-*b*-PGMA₁₉-*b*-PF-*b*-PGMA₁₉-*b*-PPO₁₅ obtained by (A) the blotting process (concentration of 20 μM polymer in water), and by (B) slow solvent evaporation at ambient conditions (concentration of 1 μM polymer in water). PF, perfluoroalkyl; PGMA, poly(glycerol monomethacrylate); PPO, poly(propylene oxide) [Color figure can be viewed at wileyonlinelibrary.com]

protocol was adopted, that is, lower copolymer concentration (1 μM) of the same sample (PPO₁₅-*b*-PGMA₁₉-*b*-PF-*b*-PGMA₁₉-*b*-PPO₁₅) was deposited onto the coated copper grid that was allowed to dry at room temperature without using a filter paper for the removal of excess solution. These filament-like structures (Figure 7(B)) are approximately 135 nm in diameter with a compact dark-gray central core of ~40 nm diameter as marked in the Figure. It could be assumed that the PF segments

segregate in the central more compact core surrounded by a less compact light gray PPO matrix that shields it from the aqueous environment during the water evaporation process.

6 | CONCLUSIONS

The synthesis of the perfluorinated bifunctional ATRP initiator (PF-initiator) was successfully carried out by reacting perfluorinated diol (PF-diol) with α-bromoisobutyryl bromide. The PF-initiator was able to polymerize SMA via ATRP that afforded well-defined Br-PSMA-*b*-PF-*b*-PSMA-Br triblock copolymers. The formed triblock copolymers were chain extended with PPO to PPO-*b*-PSMA-*b*-PF-*b*-PSMA-*b*-PPO pentablock copolymer by applying Cu(I) catalyzed azide-alkyne CuAAC chemistry after transforming Br-PSMA-*b*-PF-*b*-PSMA-Br into N₃-PSMA-*b*-PF-*b*-PSMA-N₃ and PPO into alkyne-terminated PPO-alkyne. The intended water soluble triphilic PPO-*b*-PGMA-*b*-PF-*b*-PGMA-*b*-PPO pentablock copolymers were achieved by acid hydrolysis of the PSMA blocks into PGMA. The structures of all the reaction intermediates and final triphilic pentablock copolymer were carefully characterized by various analytical tools.

Thermal analysis of the PF-initiator by DSC revealed a solid–solid phase transition at 63°C before the crystal melting at 95°C. This was also confirmed by POM and temperature-dependent WAXS studies. They also confirmed the formation of a highly crystalline lamellar structure by the PF-initiator in thin films. In contrast, the block copolymers form phase separated amorphous domains.

TEM of triphilic PPO₁₅-*b*-PGMA₁₉-*b*-PF-*b*-PGMA₁₉-*b*-PPO₁₅ pentablock copolymer after transferring the aqueous 20 μM solution to the coated copper grid and fast removal of excess solution by blotting with filter paper revealed spherical aggregates with several phase separated dark regions enriched with PF segments embedded in the PPO matrix. On the contrary, the formation of filament-like structures was observed when a 1 μM polymer solution was transferred to the copper grid that was allowed to dry at room temperature. The filament-like structure consists of a dark-gray central core that is assigned to phase segregation of PF segments surrounded by light gray regions predominantly composed of PPO segments.

ACKNOWLEDGMENTS

The authors thank Deutsche Forschungsgemeinschaft for financial support via Forschergruppe, FOR-1145. Hazrat Hussain thanks the Alexander von Humboldt Foundation

–Germany (Georg Forster Research Fellowship). Open access funding enabled and organized by Projekt DEAL. Open access funding enabled and organized by Projekt DEAL.

ORCID

Annette Meister  <https://orcid.org/0000-0003-1668-4382>

Karsten Busse  <https://orcid.org/0000-0003-4168-0957>

Jörg Kressler  <https://orcid.org/0000-0001-8571-5985>

REFERENCES

- [1] H. Cui, Z. Chen, S. Zhong, K. L. Wooley, D. J. Pochan, *Science* **2007**, *317*, 647.
- [2] S. O. Kyeremateng, T. Henze, K. Busse, J. Kressler, *Macromolecules* **2010**, *43*, 2502.
- [3] E. Amado, J. Kressler, *Soft Matter* **2011**, *7*, 7144.
- [4] J. N. Marsat, M. Heydenreich, E. Kleinpeter, H. Berlepsch, C. V. Böttcher, A. Laschewsky, *Macromolecules* **2011**, *44*, 2092.
- [5] I. W. Wyman, G. Liu, *Polymer* **2013**, *54*, 1950.
- [6] L. I. Kaberov, B. Verbraeken, M. Hruba, A. Riabtseva, L. Kovacic, S. Kereiche, J. Brus, P. Stepanek, R. Hoogenboom, S. K. Filippov, *Eur. Polym. J.* **2017**, *88*, 645.
- [7] E. H. Discekici, A. Anastasaki, R. Kaminker, J. Willenbacher, N. P. Truong, C. Fleischmann, B. Oschmann, D. J. Lunn, J. R. de Alaniz, T. P. Davis, C. M. Bates, C. J. Hawker, *J. Am. Chem. Soc.* **2017**, *139*, 5939.
- [8] A. Anastasaki, B. Oschmann, J. Willenbacher, A. Melker, M. H. C. Van Son, N. P. Truong, M. W. Schulze, E. H. Discekici, A. J. McGrath, T. P. Davis, C. M. Bates, C. J. Hawker, *Angew. Chem. Int. Ed.* **2017**, *56*, 14483.
- [9] S. Li, J. He, M. Zhang, H. Wang, P. Ni, *Polym. Chem.* **2016**, *7*, 1773.
- [10] A. A. Steinschulte, B. Schulte, S. Rütten, T. Eckert, J. Okuda, M. Möller, S. Schneider, O. V. Borisov, F. A. Plamper, *Phys. Chem. Chem. Phys.* **2014**, *16*, 4917.
- [11] A. O. Moughton, M. A. Hillmyer, T. P. Lodge, *Macromolecules* **2012**, *45*, 2.
- [12] Z. Zhou, Z. Li, Y. Ren, M. A. Hillmyer, T. P. Lodge, *J. Am. Chem. Soc.* **2003**, *125*, 10182.
- [13] D. Heinz, E. Amado, J. Kressler, *Polymers* **2018**, *10*, 960.
- [14] K. Skrabania, H. Berlepsch, C. V. Böttcher, A. Laschewsky, *Macromolecules* **2010**, *43*, 271.
- [15] J. N. Marsat, F. Stahlhut, A. Laschewsky, H. V. Berlepsch, C. Böttcher, *Colloid Polym. Sci.* **2013**, *291*, 2561.
- [16] Z. B. Li, E. Kesselman, Y. Talmon, M. A. Hillmyer, T. P. Lodge, *Science* **2004**, *306*, 98.
- [17] S. S. Guterres, M. P. Alves, A. R. Pohlmann, *Drug Target Insights* **2007**, *2*, 147.
- [18] K. Skrabania, A. Laschewsky, H. V. Berlepsch, C. Böttcher, *Langmuir* **2009**, *25*, 7594.
- [19] Z. B. Li, M. A. Hillmyer, T. P. Lodge, *Langmuir* **2006**, *22*, 9409.
- [20] J. Du, R. K. O'Reilly, *Chem. Soc. Rev.* **2011**, *40*, 2402.
- [21] X. Li, Y. Yang, G. Li, S. Lin, *Polym. Chem.* **2014**, *5*, 4553.
- [22] S. O. Kyeremateng, K. Busse, J. Kohlbrecher, J. Kressler, *Macromolecules* **2011**, *44*, 583.
- [23] S. Kubowicz, J. F. Baussard, J. F. Lutz, A. F. Thünemann, H. V. Berlepsch, A. Laschewsky, *Angew. Chemie-Int. Ed.* **2005**, *44*, 5262.
- [24] C. Liu, M. A. Hillmyer, T. P. Lodge, *Langmuir* **2008**, *24*, 12001.
- [25] T. P. Lodge, A. Rasdal, Z. Li, M. A. Hillmyer, *J. Am. Chem. Soc.* **2005**, *127*, 17608.
- [26] S. Houvenagel, L. Moine, G. Picheth, C. Dejean, A. Brûlet, A. Chennevière, V. Faugeras, N. Huang, O. Couture, N. Tsapis, *Biomacromolecules* **2018**, *19*, 3244.
- [27] L. I. Kaberov, B. Verbraeken, A. Riabtseva, J. Brus, A. Radulescu, Y. Talmon, P. Stepanek, R. Hoogenboom, S. K. Filippov, *Macromolecules* **2018**, *51*, 6047.
- [28] A. F. Thünemann, S. Kubowicz, H. V. Berlepsch, H. Möhwald, *Langmuir* **2006**, *22*, 2506.
- [29] J. He, P. Ni, C. Liu, *J. Polym. Sci. Part A Polym. Chem.* **2008**, *46*, 3029.
- [30] S. O. Kyeremateng, E. Amado, A. Blume, J. Kressler, *Macromol. Rapid Commun.* **2008**, *29*, 1140.
- [31] K. Parkatzidis, H. S. Wang, N. P. Truong, A. Anastasaki, *Chem* **2020**, *6*, 1.
- [32] N. J. Treat, H. Sprafke, J. W. Kramer, P. G. Clark, B. E. Barton, J. Read de Alaniz, B. P. Fors, C. J. Hawker, *J. Am. Chem. Soc.* **2014**, *136*, 16096.
- [33] G. M. Miyake, J. C. Theriot, *Macromolecules* **2014**, *47*, 8255.
- [34] J. Xu, K. Jung, A. Atme, S. Shanmugam, C. Boyer, *J. Am. Chem. Soc.* **2014**, *136*, 5508.
- [35] A. Moreno, J. C. Ronda, V. Cádiz, M. Galià, V. Percec, G. Lligadas, *Macromolecules* **2020**, *53*, 7285.
- [36] W. R. Dolbier, *Guide to Fluorine NMR for Organic Chemists*, John Wiley & Sons, Inc, Hoboken, NJ **2009**, Ch 6, p. 198.
- [37] W. R. Dolbier, *Guide to fluorine NMR for Organic Chemists*, John Wiley & Sons, Inc, Hoboken, NJ **2009**, Ch 2, p. 20.
- [38] R. Schwarz, J. Seelig, B. Künnecke, *Magn. Reson. Chem.* **2004**, *42*, 512.
- [39] E. Amado, J. Kressler, *Macromol. Chem. Phys.* **2005**, *206*, 850.
- [40] G. Cavallo, G. Terraneo, A. Monfredini, M. Saccone, A. Priimagi, T. Pilati, G. Resnati, P. Metrangolo, D. W. Bruce, *Angew. Chemie - Int. Ed.* **2016**, *55*, 6300.
- [41] D. Lose, S. Diele, G. Pelzl, E. Dietzmann, W. Weissflog, *Liq. Cryst.* **1998**, *24*, 707.
- [42] S. Diele, D. Lose, H. Kruth, G. Pelzl, F. Guittard, A. Cambon, *Liq. Cryst.* **1996**, *21*, 603.
- [43] M. Alaasar, M. Prehm, S. Poppe, C. Tschierske, *Chem.-A Eur. J.* **2017**, *23*, 5541.
- [44] H. Nakahara, S. Nakamura, Y. Okahashi, D. Kitaguchi, N. Kawabata, S. Sakamoto, O. Shibata, *Colloids Surfaces B Bio-interfaces* **2013**, *102*, 472.
- [45] T. Hasegawa, *Chem. Phys. Lett.* **2015**, *627*, 64.
- [46] M. Tsuji, T. Inoue, O. Shibata, *Colloids Surfaces B Bio-interfaces* **2008**, *61*, 61.
- [47] B. Heise, H. G. Kilian, F. H. Müller, *Kolloid-Zeitschrift Zeitschrift für Polym.* **1966**, *213*(1–2), 12.
- [48] J. Chen, M. Liu, H. Gong, Y. Huang, C. Chen, *Phys. Chem. B* **2011**, *115*, 14947.
- [49] H. Bao, L. Li, H. Gan, Y. Ping, J. Li, P. Ravi, *Macromolecules* **2010**, *43*, 5679.

- [50] C. P. Jesson, V. J. Cunningham, M. J. Smallridge, S. P. Armes, *Macromolecules* **2018**, *51*, 3221.
- [51] E. Amado, A. Blume, J. Kressler, *React. Funct. Polym.* **2009**, *69*, 450.
- [52] A. V. Kabanov, I. R. Nazarova, I. V. Astafieva, E. V. Batrakova, V. Y. Alakhov, A. A. Yaroslavov, V. A. Kabanov, *Macromolecules* **1995**, *28*, 2303.
- [53] M. Pulst, M. H. Samiullah, U. Baumeister, M. Prehm, J. Balko, T. Thurn-Albrecht, K. Busse, Y. Golitsyn, D. Reichert, J. Kressler, *Macromolecules* **2016**, *49*, 6609.
- [54] T. P. Russell, J. K. Rabolt, R. J. Twieg, R. L. Siemens, B. L. Farmer, *Macromolecules* **1986**, *19*, 1135.
- [55] Y. A. Lebedev, Y. M. Korolev, V. M. Polikarpov, L. N. Ignat'ev, E. M. Antipov, *Crystallogr. Rep.* **2010**, *55*, 609.
- [56] L. Guo, D. Li, H. Lennholm, H. Zhai, M. Ek, *Cellulose* **2019**, *26*, 4853.

SUPPORTING INFORMATION

Additional supporting information may be found online in the Supporting Information section at the end of this article.

How to cite this article: Heinz D, Meister A, Hussain H, Busse K, Kressler J. Triphilic pentablock copolymers with perfluoroalkyl segment in central position. *J Polym Sci.* 2020;58: 3322–3335. <https://doi.org/10.1002/pol.20200582>